Journal of Turbulence

ISSN: (Print) (Online) Journal homepage: https://www.tandfonline.com/loi/tjot20

Cyclone–anticyclone asymmetry in rotating thin fluid layers

G. Boffetta, F. Toselli, M. Manfrin & S. Musacchio

To cite this article: G. Boffetta, F. Toselli, M. Manfrin & S. Musacchio (2021) Cyclone–anticyclone asymmetry in rotating thin fluid layers, Journal of Turbulence, 22:4-5, 242-253, DOI: 10.1080/14685248.2020.1855352

To link to this article: https://doi.org/10.1080/14685248.2020.1855352

JOURNAL OF TURBULENCE
2021, VOL. 22, NOS. 4–5, 242–253
https://doi.org/10.1080/14685248.2020.1855352

Taylor & Francis
Taylor & Francis Group

Cyclone–anticyclone asymmetry in rotating thin fluid layers

G. Boffetta, F. Toselli, M. Manfrin and S. Musacchio

Dipartimento di Fisica and INFN, Università di Torino, Torino, Italy

ABSTRACT

We report of a series of laboratory experiments and numerical simulations of freely decaying rotating turbulent flows confined in domains with variable height. We show that the vertical confinement has important effects on the formation of large-scale columnar vortices, the hallmark of rotating turbulence, and in particular delays the development of the cyclone–anticyclone asymmetry. We compare the experimental and numerical results face-to-face, showing the robustness of the results.

ARTICLE HISTORY
Received 31 July 2020
Accepted 17 November 2020

KEYWORDS
Rotating turbulence; two-dimensional turbulence; cyclone–anticyclone asymmetry

1. Introduction

A distinctive feature of turbulent rotating flows is the spontaneous formation of coherent columnar vortices aligned in the direction of the rotation axis. The presence of these long-living, quasi-two-dimensional structures has been observed both in experiments [1–4] and in numerical simulations [5–9]. The mechanisms which cause their formation, in particular concerning the interplay between inertial waves and nonlinear triadic interactions, have been the subject of intense studies (for a recent review see, e.g. [10]).

Remarkably, most of these vortices are always co-rotating with the flow, i.e. they are cyclones. The predominance of cyclones over anticyclones have been reported and investigated in a large number of numerical and experimental studies, both in freely decaying turbulence [4,5,11–15] and forced turbulence [9,16–18]. It has been observed also in atmospheric measurements [19,20] and in rotating thermal convection [21–23]. The symmetry breaking is typically quantified in terms of the skewness $S_\omega = \langle \omega_z^3 \rangle / \langle \omega_z^2 \rangle^{3/2}$ of the vorticity ω_z in the direction of the rotation vector $\boldsymbol{\Omega} = \Omega \boldsymbol{e}_z$. Other indicators have been recently introduced, including third-order two-point velocity correlation functions [18], the skewness of the azimuthal velocity increments [24] and the alignment statistics between vorticity and the rotation vector [25].

Two types of arguments have been proposed to explain this phenomenon. First, cyclones have a larger vortex stretching $(2\Omega + \omega_z)\partial u_z/\partial z$ in a rotating flow with given vertical strain $\partial u_z/\partial z$. As a consequence, an isotropic turbulent flow suddenly put into rotation develops a positive skewness S_ω [26]. The second type of explanations is based on the Rayleigh

CONTACT G. Boffetta guido.boffetta@unito.it Dipartimento di Fisica and INFN, Università di Torino, via P. Giuria 1, Torino 10125, Italy

stability criterion, which shows that anticyclonic vortices are more subject to centrifugal instabilities [5,27].

Previous studies have shown that the asymmetry is strongly dependent on the Rossby number Ro. In particular, it is maximum for Ro of order unity [11]. In decaying rotating flows the skewness S_ω grows in time as Ro decreases from an initial large value [4,13,25]. A recovery of the symmetry has been observed in the late stage of the decay, when $Ro \ll 1$ [4,13]. Much less is known about the dependence of the asymmetry on the height H of the fluid in the direction of the rotation axis, because this phenomenon is typically studied in domains with the aspect ratio of order unity. Recently, it has been shown that the confinement of the flow in a thin layer causes a reduction of the asymmetry in forced rotating turbulence [24].

The aim of this paper is to investigate by means of experiments and numerical simulations of freely decaying rotating turbulence how the cyclone–anticyclone asymmetry is affected by the thickness of the flow. This issue is closely connected to the puzzling relation between rotation and two-dimensionalisation in turbulence. On the one hand, it is well known that rotation induces a two-dimensionalisation of turbulent flow, which becomes almost invariant along the rotation vector $\mathbf{\Omega}$. On the other hand, the Coriolis force affects the dynamics of the velocity field only if the latter has non-vanishing gradients in the direction of $\mathbf{\Omega}$. In particular, in a perfectly two-dimensional (2D) flow the effects of rotation disappear because the Coriolis force is cancelled by pressure gradients. Considering that the reduction of the thickness H of the layer enhances the two-dimensionalisation of the flow [24], we expect that also the cyclone–anticyclone asymmetry should be suppressed by the confinement. is not intended to reproduce exactly the same physical set-up. Our aim is to compare two systems with structural differences related to their boundary conditions. In the experiment, the turbulent flow is subject to friction with the bottom wall of the tank, which causes the development of an Ekman layer. In the numerics the boundary conditions are periodic in all directions and the bottom friction is absent. In the numerical simulations the large-scale energy transfer induced by rotation and vertical confinement [24] eventually leads to the phenomenon of spectral condensation at the horizontal scale of box. In the experiments this phenomenon does not occur because the turbulent flow is surrounded by still fluid and the diameter of the tank is much larger than the typical size of the vortices generated by the comb. Despite these differences, we show that the effects of the vertical confinement on the cyclone–anticyclone asymmetry is similar: it causes a retardation of the growth of S_ω.

2. Experimental set-up and procedure

The experiments have been performed in the rotating tank of the TurLab facility in Turin. The tank has a diameter of 5 m and it rotates anticlockwise with periods that range from 90 to 3 s. In the experiment the period of rotation was set to $T = 17.6$ s, corresponding to an angular velocity $\Omega = 2\pi/T = 0.357$ rad/s.

The tank has been filled with fresh water at four different heights $H = (10, 16, 24, 32)$ cm. Water is seeded with polyamide particles (Arkema Orgasol) with a density of 1.03 g/cm^3 and diameter $d = 20 \pm 2\,\mu$m, which are used for the visualisation of the flow using the Particle Image Velocimetry technique. The particles are illuminated by an horizontal laser sheet, at 6 cm above the floor of the tank, generated by a Quantum Opus solid state

diode green laser. The images are acquired by a 8-bits camera Dalsa Falcon 4M60 with 2352×1728 pixels resolution (further details of the tank and of the acquisition system can be found in [28]). The camera is located 1.43 m above the horizontal laser sheet.

Before the beginning of the experiment, the fluid is set to solid body rotation by increasing gradually the angular velocity of the tank. Then, trails of vortices are generated by the horizontal motion of a comb, which is mounted on a motorised linear guide. The comb is composed of six vertical flat plates of width $a = 2.3$ cm with a mesh size of $M = 10$ cm. It moves with constant velocity $V = 18$ cm/s over a distance $L = 90$ cm. In order to avoid the formation of waves, the velocity of the comb is smoothly reduced to zero close to the extremities of the guide, before inverting the direction of motion. The comb Reynolds and Rossby numbers, defined in terms of the comb velocity V and the mesh spacing M as in [4], are $Re_c = VM/\nu = 1.8 \times 10^4$ and $Ro_c = V/(2\Omega M) = 2.5$. A schematic of the experimental set-up is represented in Figure 1.

After 10 min of initial forcing, the comb is stopped and the decay of the flow is recorded for 1 min with an acquisition rate of 60 Hz. The forcing is resumed for a duration of 2 min and then stopped before the next recording. The procedure is repeated 15 times for each height H of the fluid layer.

The velocity fields are obtained by standard PIV analysis, using the Open Source Particle Image Velocimetry software (OpenPIV, for more detail see [29]) with an interrogation window of 32×32 pixels size and an overlap of 16 pixels. The resulting velocity fields cover a rectangular area of size $L_x = 28$ cm and $L_y = 20.5$ cm and are defined on a grid of 116×85 points with a uniform spatial resolution of $\Delta x = \Delta y = 0.241$ cm. We reconstructed the velocity fields with a sampling rate of 0.1 s, skipping an initial time of 0.5 s from the last passage of the comb to avoid the disturbances of the free surface.

The measured velocity fields are the superposition of the turbulent fields $\boldsymbol{u}(\boldsymbol{x}, t)$ and a uniform velocity $\boldsymbol{U}(t)$ which is due to the large-scale circulation induced by the comb and the inertial waves. The inertial waves manifest in the time series of $U_x(t)$ and $U_y(t)$ as oscillations with a period which is half of the rotation period of the tank $T_{IW} = T/2$ and a phase shift of $\pi/2$ between U_x and U_y. Before proceeding to the analysis of the data we have subtracted the uniform velocity $\boldsymbol{U}(t)$ (as in [4]).

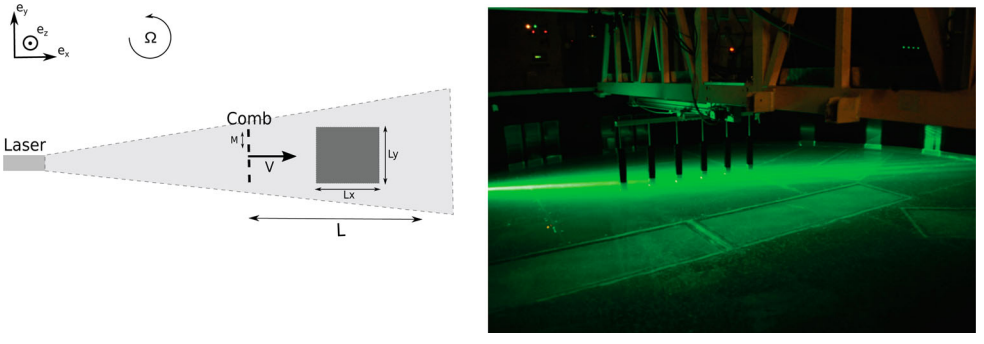

Figure 1. Left panel: schematic of the experimental set-up. Right panel: photo of the experimental set-up.

The time series presented in Section 4 is first averaged at a fixed time over the ensemble of 15 experiments at a given height and further time-averaged over a window of 1 s. The experimental data have been nondimensionalised using the comb scale M, the rms horizontal velocity at initial time $u_0 = \langle (u_x^2 + u_y^2)/2 \rangle^{1/2}(t = 0)$ and the timescale $T_0 = M/u_0$.

3. Numerical simulations

Besides the experiments, we also performed a series of direct numerical simulations (DNS) of an incompressible velocity field in a rotating domain with variable height. The dynamics of the velocity field $\boldsymbol{u}(\boldsymbol{x}, t)$ is described by the rotating Navier–Stokes equation:

$$\partial_t \boldsymbol{u} + \boldsymbol{u} \cdot \boldsymbol{\nabla} \boldsymbol{u} + 2\boldsymbol{\Omega} \times \boldsymbol{u} = -\frac{\boldsymbol{\nabla} p}{\rho} + \nu \nabla^2 \boldsymbol{u} \tag{1}$$

where $\Omega = (0, 0, \Omega)$ is the angular velocity of the reference frame, ρ is the uniform density of the fluid, ν is the kinematic viscosity and the pressure p is determined by the condition $\nabla \cdot \mathbf{u} = 0$.

We perform the DNS by means of a standard 2/3-dealiased, pseudospectral code with second-order Runge–Kutta integration scheme. The velocity field is defined on a triply periodic domain with fixed horizontal sizes $L_x = L_y = 2\pi$ and variable height $H = (1/4, 1/2, 1) \times 2\pi$. It is discretized on a uniform grid at resolution $N_x = N_y = (H/L_x)N_z = 512$. For each height H, we consider two values of the angular velocity $\Omega = (1, 2)$. The viscosity is set to $\nu = 10^{-3}$.

At time $t = 0$, the velocity field is initialised as the superposition of a large-scale two-dimensional, two-component (2D2C) flow, and a small three-dimensional, three-component (3D3C) perturbation. The 2D2C large-scale flow mimics the 2D vortices generated by the comb in the experiment. Nonetheless, it is worth to notice that the initial flows in the DNS and experiments are not identical. In the DNS the small 3D perturbation requires some time to develop the 3D turbulent flow. In the experiments, 3D turbulence is already present in the initial flow as a result of the previous passages of the comb. The velocities u_x and u_y of the 2D2C flow are defined in Fourier space as the sum of random Gaussian horizontal modes $(k_x, k_y, k_z = 0)$ with $k_h = (k_x^2 + k_y^2)^{1/2}$ in the range $4 < k_h < 6$. The 3D3D perturbation is defined in the Fourier space as the sum of random Gaussian modes in the shell $2 < |\boldsymbol{k}| < 8$. The amplitude of the perturbation field is 5×10^{-4} smaller than the 2D2C flow.

For each height H we performed 10 simulations with different initial random flow, keeping constant the kinetic energies of the base flow and of the perturbation. The time series presented in Section 4 is obtained from the ensemble average at fixed time of the data obtained in the 10 simulations with given H. The data of the DNS are nondimensionalised using the scale $L_0 = 2\pi/4$, corresponding to the largest wavelength of the initial flow, the rms horizontal velocity at initial time $u_0 = \langle (u_x^2 + u_y^2)/2 \rangle^{1/2}(t = 0)$, ($u_0 = 0.93$ for all (H, Ω)) and the timescale $T_0 = L_0/u_0$.

4. Experimental and numerical results

In Figure 2 we show two examples of the typical vorticity fields obtained in the experiments and in the DNS. More precisely, the left panel shows a square portion (with size $L_y \times L_y$) of the vertical vorticity field $\omega_z = \partial_x u_y - \partial_y u_x$ at time $t = 1.8T_0$ in the experiments at $H = 32$ cm, while the right panel shows a section at $z = 0$ of the vertical vorticity field $\omega_z(x, y, z = 0)$ at time $t = 7.1T_0$ in the simulations at $H = \pi/2$ and $\Omega = 1$. In both the experiments and the DNS it is clearly visible the presence of Large observable vortices are all cyclonic (in red).

The formation of these structures during the decay of the rotating flow causes an increase of the horizontal correlation scale. In order to quantify this effect we first compute the longitudinal correlation function of horizontal velocity $C(r, t) = \langle u_\alpha(\boldsymbol{x}, t) u_\alpha(\boldsymbol{x} + r\boldsymbol{e}_\alpha, t)\rangle / \langle u_\alpha(\boldsymbol{x}, t)^2\rangle$ with $\alpha = (x, y)$. Then we define the correlation length $L_c(t)$ as the scale at which $C(L_c) = 0.8$. The time evolution of L_c is shown in Figure 3. In both the experiments and the DNS we observe a weak dependence of L_c on H. The scale L_c increases almost linearly in time for $t > T_0$. Previous studies have reported a different scaling $L_c(t) \simeq t^\beta$ with exponent β in the range $(0.2, 0.4)$ [4,30]. We note that the growth of L_c is faster in the DNS than in the experiments: in the DNS the average growth rate of L_c is $L_c/L_0 \simeq 0.05t/T_0$, while in the experiments it is $L_c/M \simeq 0.03t/T_0$. This effect could be caused by the 2D2C initial condition in the DNS, which induces a 2D dynamics characterised by stronger large-scale energy transfer.

The growth of the correlation scale influences the time evolution of the Reynolds and Rossby numbers, defined as

$$Re(t) = \frac{u_h L_c}{\nu}, \quad Ro(t) = \frac{u_h}{2\Omega L_c}, \tag{2}$$

where u_h is the rms horizontal velocity $u_h = (\langle (u_x^2 + u_y^2)/2\rangle^{1/2})$. As shown in Figure 4 (left panel), in the experiments, after an initial rapid decay at $t < T_0$, the Reynolds number

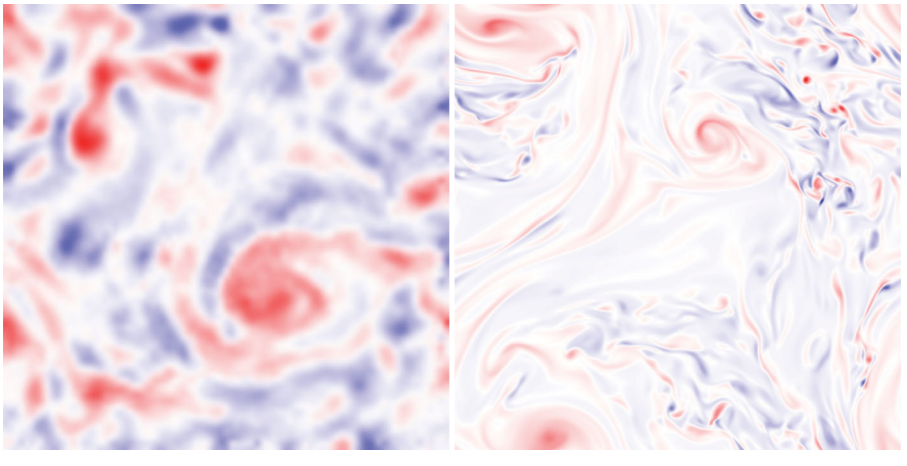

Figure 2. Vertical vorticity field in the experiments with $H = 32$ cm at time $t = 1.8T_0$ (left panel) and in the DNS with $H = \pi/2$ and $\Omega = 1$ at time $t = 7.1T_0$ (right panel). Cyclonic vortices are represented in red.

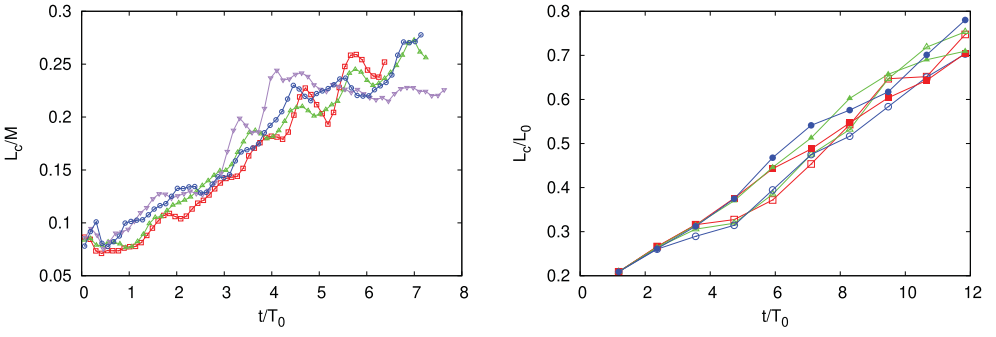

Figure 3. Left panel: velocity correlation length L_c in the experiments at $\Omega = 0.357$ rad/s with $H = 10$ cm (red squares), $H = 16$ cm (green triangles), $H = 24$ cm (purple down-pointing triangles) and $H = 32$ cm (blue circles). Right panel: Velocity correlation length L_c in the DNS with $H = \pi/2$ (red squares), $H = \pi$ (green triangles) and $H = 2\pi$ (blue circles) at angular velocity $\Omega = 1$ (empty symbols) and $\Omega = 2$ (filled symbols).

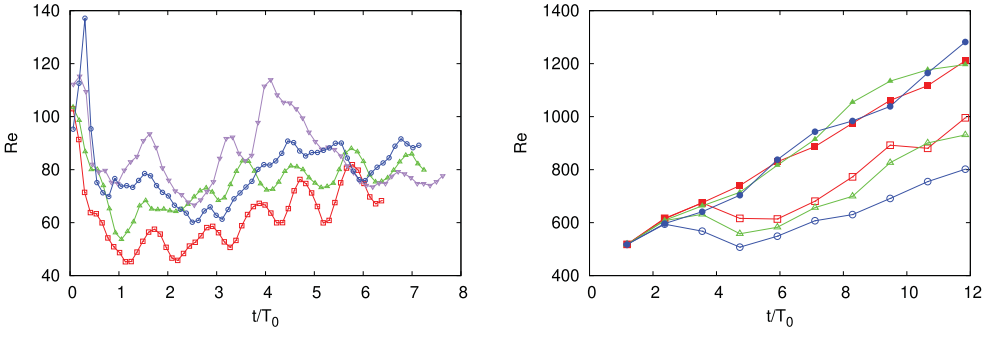

Figure 4. Reynolds number $Re = L_c u_{rms}/\nu$ in the experiments (left panel) and in the DNS (right panel) at angular velocity $\Omega = 1$ (empty symbols) and $\Omega = 2$ (filled symbols). Symbols as in Figure 3.

remains approximatively constant with some fluctuations (similar to what was observed in [4]). Conversely, in the DNS we observe an almost linear increase of $Re(t)$, which indicates that the growth of $L_c(t)$ overwhelms the decay of the velocities. We argue that the difference between the behaviour of two systems could be ascribed to their different boundary conditions. In the experiments the bottom friction (which is absent in the DNS) causes a faster decay of the velocities, resulting in a different temporal evolution of Re. The dependence of $Re(t)$ on H is unclear: in the experiments with the thinner layer ($H = 10$ cm) the values of Re are on average smaller than those measured with the thickest layer ($H = 32$ cm), but we observe the opposite behavior in the DNS with $\Omega = 1$.

The Rossby number decreases in time both in the experiments and in the numerics (see Figure 5) and it is almost independent of H. At long times $t > T$ we observe a scaling regime $Ro(t) \simeq t^{-1}$. This scaling has been previously reported in [4]. The decay of the Rossby number indicates that the Coriolis force prevails over the inertial forces at long times. Therefore, the effects of rotation are expected to become more pronounced as the system evolves.

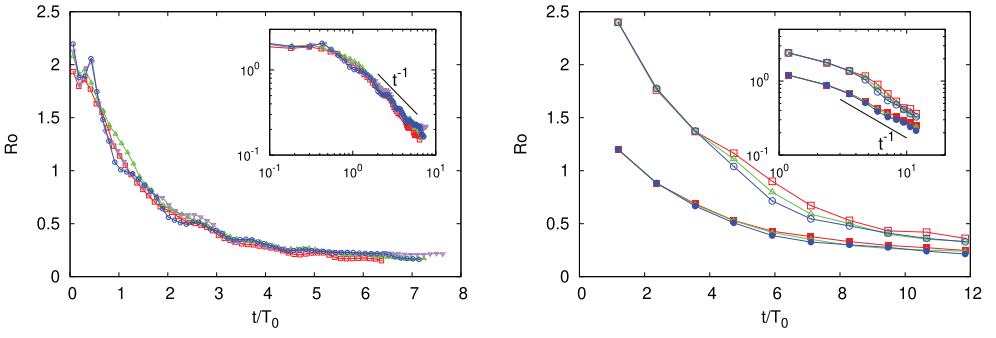

Figure 5. Rossby number $Ro = u_{rms}/2\Omega L_c$ in the experiments (left panel) and in the DNS (right panel) at angular velocity $\Omega = 1$ (empty symbols) and $\Omega = 2$ (filled symbols). Symbols as in Figure 3.

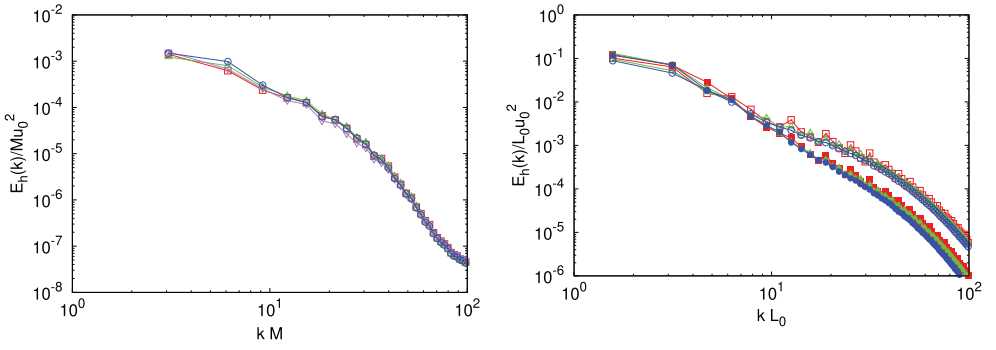

Figure 6. Horizontal energy spectra in the experiments at time $t = 1.8T_0$ (left panel) and in the DNS at time $t = 7.1T_0$ (right panel) at angular velocity $\Omega = 1$ (empty symbols) and $\Omega = 2$ (filled symbols). Symbols as in Figure 3.

In Figure 6 we compare the energy spectra $E_h(k)$ of the horizontal velocity fields u_x, u_y in the experiments at $t = 1.8T_0$ (left panel) and in the DNS at time $t = 7.1T_0$ (right panel). In the experiments we observe a power-law spectrum $E_h(k) \simeq k^{-2}$ in the wavenumber range $6 < kM < 20$. A similar spectral slope is observed also in the DNS at $\Omega = 1$ in the range $10 < kL_0 < 30$, while the simulations with $\Omega = 2$ have steeper spectra. In both the experiments and DNS the spectra are almost independent of the heights H. In the spectra of the DNS it is possible to observe a beginning of accumulation of energy in the lowest accessible mode. The spectral condensation is clearly visible in the spectra at late times of the DNS (not shown). Conversely, this phenomenon is not observed in the experiments because of the large-scale separation between the diameter of the tank and the typical size of the vortices produced by the comb.

The results presented so far do not show a strong dependence on the height of the fluid layer. On the contrary, the effect of varying H is clearly visible in the statistics of the vertical component of the vorticity $\omega_z = \partial_x u_y - \partial_y u_x$. The probability distribution functions (PDF) of ω_z are shown in Figure 7 for different values of H at a fixed time $t = 1.8T_0$ in the experiments and $t = 7.1T_0$ in the DNS. The PDFs corresponding to the large H are characterised by a positive skewness $S_\omega = \langle \omega_z^3 \rangle / \langle \omega_z^2 \rangle^{3/2}$, which quantifies the cyclone–anticyclone asymmetry. Reducing the thickness H, the PDFs become more

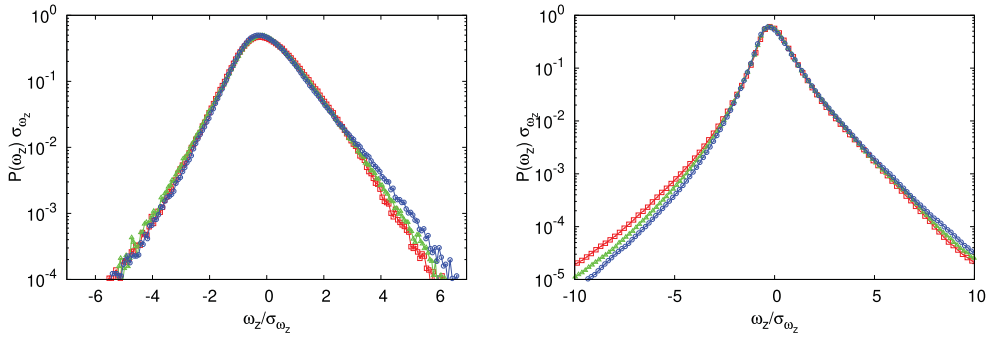

Figure 7. PDFs of the vertical vorticity ω_z in the experiments at time $t = 1.8T_0$ (left panel) and in the DNS at time $t = 7.1T_0$ at angular velocity $\Omega = 1$ (right panel). Symbols as in Figure 3.

symmetric and the skewness is reduced. This means that the confinement of the decaying flow in a thin layer weakens the cyclone–anticyclone asymmetry at a fixed time. This is in qualitative agreement with previous numerical results in forced stationary conditions [24].

Because of the decay of the Rossby number, it is expected that the cyclone–anticyclone asymmetry increases with time. Previous studies[4,25] reported a power-law growth of the skewness $S_\omega \simeq t^\gamma$ with $\gamma \approx 0.70 \pm 0.05$. Here, we are interested to investigate how the height H of the fluid layer influences the growth of S_ω. The temporal evolution of S_ω is shown in Figure 8. In all the simulations and experiments, after an initial transient we observe the development of a positive skewness, which indicates the prevalence of cyclones over anticyclones. In the DNS, we find that the regime of positive skewness is systematically preceded by a transient in which S_ω is negative. We are not aware of previous observations of this phenomenon. After the negative transient, the skewness in the DNS grows as $S_\omega(t) \sim (t - t_*)^{0.80\pm0.05}$ (not shown), t_* being the time at which S_ω changes sign from negative to positive. The value of the exponent is in agreement with the results reported in [25].

The series of $S_\omega(t)$ obtained in the numerics display a clear dependence on H. Smaller H corresponds to smaller values of S_ω at a fixed short time. A similar dependence on H is observed also in the experimental series, even if they are more noisy. After the initial growth, the skewness saturates to almost constant values at late times both in the DNS (for $t > 8T_0$) and experiments (for $t > 4T_0$). In the numerical series with $\Omega = 2$, the asymptotic value of the skewness has not a clear dependence on H. In the experiments with $H = 24$ cm we observe a decay of S_ω at $t > 5T_0$. It is tempting to interpret this as the beginning of the long time decay of the vorticity skewness which has been reported in previous studies (e.g. [4]). Nonetheless, even after averaging over 15 independent experiments, our data display strong temporal fluctuations which do not allow to make accurate statements concerning the late stage of the evolution of the skewness. The inspection of the numerical series in Figure 8 suggests that while the cyclone–anticyclone asymmetry develops for all the cases with different H considered here, reaching similar values of S_ω at the end of the simulations, the main effect of the confinement of the flow in a thin layer is to retard its development. To test this idea, in Figure 9 we plot the series of $S_\omega(t)$ by rescaling the times with height-dependent time scales T_H. The values of T_H have been determined by the least square method, minimising the differences between $S_\omega(t/T_H)$ at given H with respect to

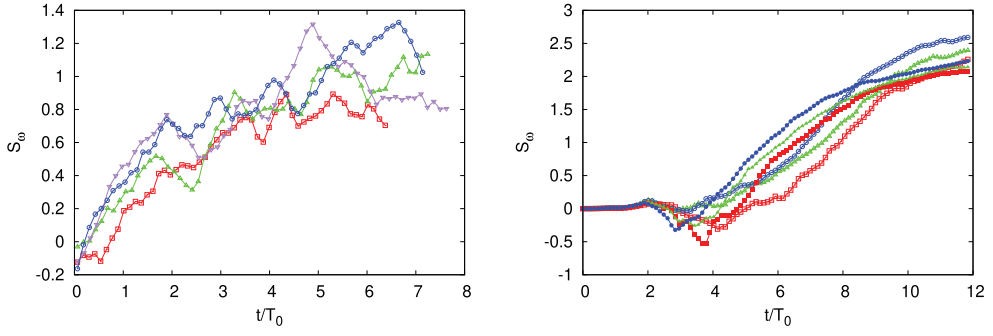

Figure 8. Skewness of the vertical vorticity ω_z in the experiments (left panel) and in the DNS (right panel) at angular velocity $\Omega = 1$ (empty symbols) and $\Omega = 2$ (filled symbols). Symbols as in Figure 3.

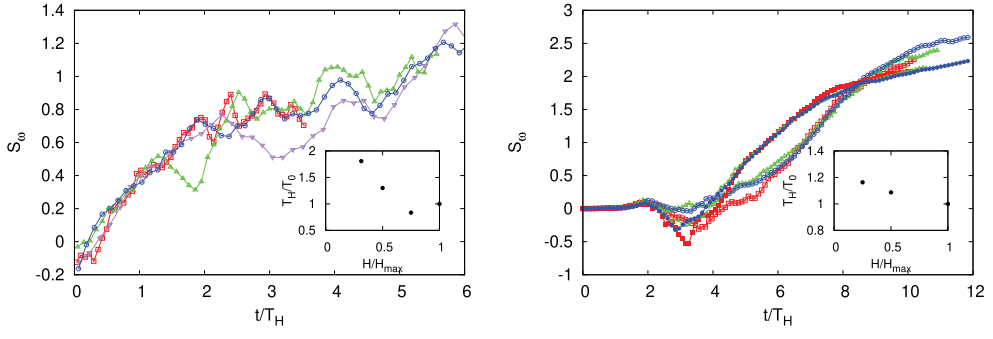

Figure 9. Skewness of the vertical vorticity ω_z in the experiments (left panel) and in the DNS (right panel) at angular velocity $\Omega = 1$ (empty symbols) and $\Omega = 2$ (filled symbols). Time has been rescaled with T_H. The values of T_H are shown in the insets. Symbols as in Figure 3.

the case with the largest $H = H_{\max}$ ($H_{\max} = 32$ cm in the experiments and $H_{\max} = 2\pi$ in the DNS), and fixing $T_{H_{\max}} = T_0$. The collapse of the series is reasonably good, and the rescaling times T_H become larger as the thickness H is reduced. We note that the values of T_H/T_0 are identical in the DNS with $\Omega = 1$ and $\Omega = 2$. This shows that the confinement in a thin layer slows down the development of the cyclone–anticyclone asymmetry. It is interesting to note that this effect is qualitatively similar in the experiment and in the DNS, in spite of the differences between the two systems highlighted in the introduction and observed in the temporal evolution of the correlation scale (Figure 3) the Reynolds number (Figure 4) and the spectra (Figure 6).

Finally, we present a result of the late-stage of the decay in the DNS. We have continued the DNS up to time $t = 24T_0$. At that time, the turbulent fluctuations almost completely disappeared, and the velocity field consists of a single cyclonic vortex. Because in the DNS the mean vorticity is constrained to be zero, the vortex is surrounded by a sea of negative vorticity. As one can see in Figure 10, the PDF of the vorticity field of this fossil state of turbulence displays an interesting feature: its negative tail has a sharp cutoff at $\omega_z = -2\Omega$. In other words, at long times the total vorticity computed in the laboratory frame $\omega_z + 2\Omega$ is always positive. This result contrasts with the recovery of the symmetry at long times which has been observed in [4,13]. As discussed in [4], the symmetry is expected to be

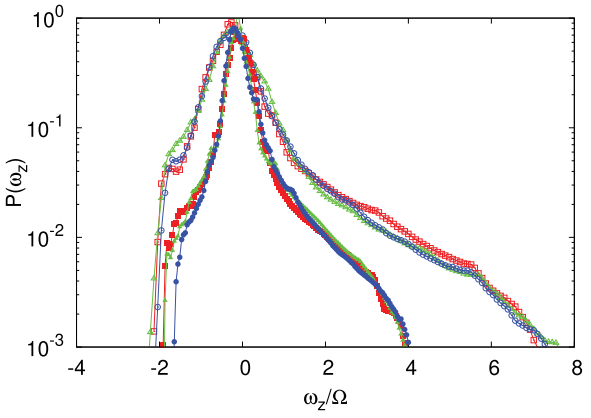

Figure 10. PDFs of the vertical vorticity ω_z in the numerical simulations at time $t = 24T_0$ at angular velocity $\Omega = 1$ (empty symbols) and $\Omega = 2$ (filled symbols). Symbols as in Figure 3.

restored only if the initial state contains a significant amount of vertical velocity, which is almost absent in our case. It would be interesting to investigate more systematically how this phenomenon is dependent on the properties of the initial velocity field and on the boundary conditions.

5. Conclusion

The main result of our study is that the confinement of a turbulent rotating flow in a thin layer delays the development of the cyclone–anticyclone asymmetry. have structural differences in the boundary conditions, and it is therefore a robust feature of decaying rotating flows, independent of the presence of bottom friction. Our findings show that although the formation of the cyclone–anticyclone asymmetry is observed both with and without vertical confinement, the height of the fluid layer is a crucial parameter to determine the temporal scale of this phenomenon. Further experiments and numerical simulations are needed to better understand how the mechanism of formation of cyclonic columnar structures is influenced by the vertical confinement.

Our results have important implication for large-scale geophysical flows, where the height of the fluid layer is typically smaller than the horizontal scales. The cyclone–anticyclone asymmetry observed in these conditions could be much weaker than what expected on the basis of experiments and DNS with aspect ratio of order unity.

Acknowledgments

We acknowledge the financial support of the project "European High performance Infrastructures in Turbulence" (EUHIT) (Grant agreement ID: 312778) in the frame of the Research Infrastructures Integrating Activity framework of FP7. We also acknowledge support by the Departments of Excellence grant (MIUR).

Disclosure statement

No potential conflict of interest was reported by the authors.

Funding

We acknowledge the financial support of the project "European High performance Infrastructures in Turbulence" (EUHIT) (Grant agreement ID: 312778) in the frame of the Research Infrastructures Integrating Activity framework of FP7.

References

[1] Hopfinger EJ, Browand FK, Gagne Y. Turbulence and waves in a rotating tank. J Fluid Mech. 1982;125:505–534.
[2] Longhetto A, Montabone L, Provenzale A, et al. Coherent vortices in rotating flows: a laboratory view. Nuovo Cimento della Societa Italiana Fisica C. 2002;25(2):233–249.
[3] Staplehurst PJ, Davidson PA, Dalziel SB. Structure formation in homogeneous freely decaying rotating turbulence. J Fluid Mech. 2008;598:81–105.
[4] Moisy F, Morize C, Rabaud M, et al. Decay laws, anisotropy and cyclone–anticyclone asymmetry in decaying rotating turbulence. J Fluid Mech. 2011;666:5–35.
[5] Bartello P, Métais O, Lesieur M. Coherent structures in rotating three-dimensional turbulence. J Fluid Mech. 1994;273:1–29.
[6] Yeung P, Zhou Y. Numerical study of rotating turbulence with external forcing. Phys Fluids. 1998;10(11):2895–2909.
[7] Smith LM, Waleffe F. Transfer of energy to two-dimensional large scales in forced, rotating three-dimensional turbulence. Phys Fluids. 1999;11(6):1608–1622.
[8] Yoshimatsu K, Midorikawa M, Kaneda Y. Columnar eddy formation in freely decaying homogeneous rotating turbulence. Fluid Mechanics¡/DIFdel¿J Fluid Mech. 2011;677:154.
[9] Biferale L, Bonaccorso F, Mazzitelli IM, et al. Coherent structures and extreme events in rotating multiphase turbulent flows. Phys Rev X. 2016;6(4):041036.
[10] Godeferd FS, Moisy F. Structure and dynamics of rotating turbulence: a review of recent experimental and numerical results. Appl Mech Rev. 2015;67(3):030802.
[11] Bourouiba L, Bartello P. The intermediate Rossby number range and two-dimensional–three-dimensional transfers in rotating decaying homogeneous turbulence. J Fluid Mech. 2007;587:139–161.
[12] Van Bokhoven LJA, Cambon C, Liechtenstein L, et al. Refined vorticity statistics of decaying rotating three-dimensional turbulence. J Turbulence. 2008;9:N6.
[13] Morize C, Moisy F, Rabaud M. Decaying grid-generated turbulence in a rotating tank. Phys Fluids. 2005;17(9):095105.
[14] Morize C, Moisy F. Energy decay of rotating turbulence with confinement effects. Phys Fluids. 2006;18(6):065107.
[15] Praud O, Sommeria J, Fincham AM. Decaying grid turbulence in a rotating stratified fluid. J Fluid Mech. 2006;547:389–412.
[16] Godeferd FS, Lollini L. Direct numerical simulations of turbulence with confinement and rotation. J Fluid Mech. 1999;393:257–308.
[17] Smith LM, Lee Y. On near resonances and symmetry breaking in forced rotating flows at moderate Rossby number. J Fluid Mech. 2005;535:111–142.
[18] Gallet B, Campagne A, Cortet PP, et al. Scale-dependent cyclone–anticyclone asymmetry in a forced rotating turbulence experiment. Phys Fluids. 2014;26(3):035108.
[19] Cho JYN, Lindborg E. Horizontal velocity structure functions in the upper troposphere and lower stratosphere: 1. observations. J Geophys Res Atmospheres. 2001;106(D10):10223–10232.
[20] Hakim GJ, Canavan AK. Observed cyclone–anticyclone tropopause vortex asymmetries. J Atmospheric Sci. 2005;62(1):231–240.
[21] Cheng JS, Stellmach S, Ribeiro A, et al. Laboratory-numerical models of rapidly rotating convection in planetary cores. Geophys J Int. 2015;201(1):1–17.
[22] Guervilly C, Huges DW, Jones CA. Large-scale vortices in rapidly rotating Rayleigh-Bénard convection. J Fluid Mech. 2014;758:407–435.

[23] Vorobieff P, Ecke RE. Vortex structure in rotating Rayleigh-Benard convection. Phys D Nonlinear Phenomena. 1998;123(1–4):153–160.
[24] Deusebio E, Boffetta G, Lindborg E, et al. Dimensional transition in rotating turbulence. Phys Rev E. 2014;90(2):023005.
[25] Naso A. Cyclone-anticyclone asymmetry and alignment statistics in homogeneous rotating turbulence. Phys Fluids. 2015;27(3):035108.
[26] Gence JN, Frick C. Naissance des corrélations triples de vorticité dans une turbulence statistiquement homogène soumise à une rotation. Comptes Rendus Acad Sci-Ser IIB-Mech. 2001;329(5):351–356.
[27] Sreenivasan B, Davidson PA. On the formation of cyclones and anticyclones in a rotating fluid. Phys Fluids. 2008;20(8):085104.
[28] Ferrero E, Mortarini L, Manfrin M, et al. Boundary-layer stress instabilities in neutral, rotating turbulent flows. Meteorology¡/DIFdel¿Boundary Layer Meteorol. 2009;130(3):347.
[29] Taylor ZJ, Gurka R, Kopp GA, et al. Long-duration time-resolved PIV to study unsteady aerodynamics. IEEE Trans Instrum Meas. 2010;59(12):3262–3269.
[30] Jacquin L, Leuchter O, Cambonxs C, et al. Homogeneous turbulence in the presence of rotation. J Fluid Mech. 1990;220:1–52.